

**An objective
multiparametric
interpretation of
palaeoseismic trench
stratigraphy**

S. Schneiderwind et al.

This discussion paper is/has been under review for the journal Solid Earth (SE).
Please refer to the corresponding final paper in SE if available.

3-D visualisation of palaeoseismic trench stratigraphy and trench logging using terrestrial remote sensing and GPR – combining techniques towards an objective multiparametric interpretation

S. Schneiderwind¹, J. Mason¹, T. Wiatr², I. Papanikolaou³, and K. Reicherter¹

¹Institute of Neotectonics and Natural Hazards, RWTH Aachen University,
Lochnerstraße 4–20, 52056 Aachen, Germany

²Fundamental matters/Division GI, Federal Agency for Cartography and Geodesy,
Richard-Strauss-Allee 11, 60598 Frankfurt am Main, Germany

³Laboratory Mineralogy – Geology, Agricultural University of Athens,
Iera Odos 75, Athens, 11855 Greece

Received: 24 August 2015 – Accepted: 30 August 2015 – Published: 22 September 2015

Correspondence to: S. Schneiderwind (s.schneiderwind@nug.rwth-aachen.de)

Published by Copernicus Publications on behalf of the European Geosciences Union.

Title Page

Abstract

Introduction

Conclusions

References

Tables

Figures

◀

▶

◀

▶

Back

Close

Full Screen / Esc

Printer-friendly Version

Interactive Discussion

Abstract

Two normal faults on the Island of Crete and mainland Greece were studied to create and test an innovative workflow to make palaeoseismic trench logging more objective, and visualise the sedimentary architecture within the trench wall in 3-D. This is achieved by combining classical palaeoseismic trenching techniques with multispectral approaches. A conventional trench log was firstly compared to results of iso cluster analysis of a true colour photomosaic representing the spectrum of visible light. Passive data collection disadvantages (e.g. illumination) were addressed by complementing the dataset with active near-infrared backscatter signal image from t-LiDAR measurements. The multispectral analysis shows that distinct layers can be identified and it compares well with the conventional trench log. According to this, a distinction of adjacent stratigraphic units was enabled by their particular multispectral composition signature. Based on the trench log, a 3-D-interpretation of GPR data collected on the vertical trench wall was then possible. This is highly beneficial for measuring representative layer thicknesses, displacements and geometries at depth within the trench wall. Thus, misinterpretation due to cutting effects is minimised. Sedimentary feature geometries related to earthquake magnitude can be used to improve the accuracy of seismic hazard assessments. Therefore, this manuscript combines multiparametric approaches and shows: (i) how a 3-D visualisation of palaeoseismic trench stratigraphy and logging can be accomplished by combining t-LiDAR and GRP techniques, and (ii) how a multispectral digital analysis can offer additional advantages and a higher objectivity in the interpretation of palaeoseismic and stratigraphic information. The multispectral datasets are stored allowing unbiased input for future (re-)investigations.

1 Introduction

Seismic hazard assessment is still predominantly based on the instrumental and historical catalogues of seismicity. However, these catalogues are generally too short com-

An objective multiparametric interpretation of palaeoseismic trench stratigraphy

S. Schneiderwind et al.

Title Page

Abstract

Introduction

Conclusions

References

Tables

Figures

◀

▶

◀

▶

Back

Close

Full Screen / Esc

Printer-friendly Version

Interactive Discussion



An objective multiparametric interpretation of palaeoseismic trench stratigraphy

S. Schneiderwind et al.

Title Page

Abstract

Introduction

Conclusions

References

Tables

Figures

◀

▶

◀

▶

Back

Close

Full Screen / Esc

Printer-friendly Version

Interactive Discussion



pared to the recurrence interval of particular faults (e.g. Wesnousky, 1986; Yeats and Prentice, 1996; Machette, 2000). As a result, the sample from the statistical elaboration of the historical and instrumental data is incomplete and a large number of faults would have not ruptured during the period where the historical record is considered complete (Grützner et al., 2013; Papanikolaou et al., 2015). The need for fault specific studies and the extraction of recurrence intervals from palaeoseismological trenches was then initiated in the late 1970s (Sieh, 1978; McCalpin, 2009). The goal is to extend the history of slip on a fault back many thousands of years, a time span that generally encompasses a large number of earthquake cycles (Yeats and Prentice, 1996).

Over the last few years fault specific studies and palaeoseismology have been further advanced and are now supported by new remote sensing tools that offer high spatial resolution (e.g. LiDAR) and geophysics that extend our data into the subsurface (Ground Penetration Radar (GPR), Electric Resistivity Tomography (ERT)) (Papanikolaou et al., 2015). This manuscript adds on such approaches and shows: (i) how a 3-D visualisation of palaeoseismic trench stratigraphy and logging can be accomplished by combining t-LiDAR and GRP techniques, and (ii) how a multispectral digital analysis can offer additional advantages and a higher objectivity in the interpretation.

Palaeoseismological studies are often undertaken to identify earthquake recurrence intervals and maximum credible magnitudes of prehistoric earthquakes (McCalpin, 2009). These parameters are needed for the accurate calculation of seismic hazard potential of active fault zones (Michetti et al., 2005; Reicherter et al., 2009). Evidence for palaeoearthquakes can be found within the sedimentary architecture of active faults where conditions are favourable for their preservation. Typical features caused by recurrent seismic events include: (i) progressive displacements (Keller and Rockwell, 1984), (ii) colluvial wedges, (iii) Liquefaction, and (iv) fissure fills (Reicherter et al., 2003; Kokkalas et al., 2007; McCalpin, 2009) (see Fig. 1vi). The geometry and stratigraphic position of these features allow the relative dating of recurrent surface rupturing events, whereas carbon rich material (usually within buried palaeosols) can be used to date prehistoric earthquakes and determine recurrence intervals. To access these

An objective multiparametric interpretation of palaeoseismic trench stratigraphy

S. Schneiderwind et al.

Title Page

Abstract

Introduction

Conclusions

References

Tables

Figures

◀

▶

◀

▶

Back

Close

Full Screen / Esc

Printer-friendly Version

Interactive Discussion

potential archives of seismic information expensive trenches are excavated across deformation zones. Then, the classical approach is to document stratigraphy and structure by careful logging, either on paper and/or with photographs (e.g. Wallace, 1986; McCalpin, 2009). The accuracy of the trench log is, however, dependent on the logger's experience and ability to define mappable units; discrete deposits that are composed of similar lithology need to be distinguished from adjacent deposits.

Palaeoseismic indicators are widely spread and their formation varies along fault strike (e.g. Bubeck et al., 2015). For this reason, geophysical surveys undertaken prior to the trenching phase have become common practice over the last decade. For instance, ground-penetrating radar (GPR) measurements have been carried out to identify optimum trenching locations (e.g. Demanet et al., 2001; Alasset and Meghraoui, 2005; Grützner et al., 2012) and many studies have shown that earthquake related structures can be identified in the shallow subsurface with geophysics (e.g. Chow et al., 2001; Reiss et al., 2003; Bubeck et al., 2015). The excavated trench is then a 2-D representation of the fault zone stratigraphy. It is assumed that the 2-D geometry of the logged sedimentary features continues along strike either side of case; without widening the trench along strike, or excavating more trenches, we must assume that the 2-D trench log is representative for this location along the fault. Trenches target predominantly palaeosols on either side of the fault, and then according to empirical relationships (Wells and Coppersmith, 1994) palaeomagnitudes can be estimated based on these co-seismic displacements. If no or only poorly expressed displaced palaeosols exist the geometry of sedimentary features within trenches is used to estimate previous earthquake displacements. As a “rule of thumb” colluvial wedge thickness equals half of the initial scarp height (e.g. Reicherter, 2001; Reiss et al., 2003; McCalpin, 2009). Such information are then used as input parameters for seismic hazard assessment. Therefore, tracing the geometry of these features is essential for the most accurate seismic hazard calculations. A better visualisation can improve the definition of separate unit boundaries and features, offering better interpretations and limiting uncertainties.

An objective multiparametric interpretation of palaeoseismic trench stratigraphy

S. Schneiderwind et al.

Title Page

Abstract

Introduction

Conclusions

References

Tables

Figures

◀

▶

◀

▶

Back

Close

Full Screen / Esc

Printer-friendly Version

Interactive Discussion



In this study we demonstrate how high-resolution t-LiDAR (terrestrial light detection and ranging) measurements and photomosaics can be used to assist in the interpretation of palaeoseismological exposures; we also show how GPR can be used to visualise sedimentary structures in 3-D within the trench wall. The t-LiDAR's backscatter signal represents material reflectance of radiation in the near-infrared wavelength, and digital photo cameras collect information of the reflectance of visible light; therefore, a quasi-multispectral inspection of the exposures is possible. Ragona et al. (2006) developed a method using imaging spectroscopy on palaeoseismic exposures with hyperspectral and normal digital cameras. As an outcome they were able to enhance the visualisation of the sedimentary layers and other features that are not obvious or even not visible to the human eye. Another study undertaken by Wiatr et al. (2015) places emphasis on the use of the monochromatic laser beam's backscattered signal to determine varying surface conditions. Using these techniques we make experienced-based trench logging more objective. GPR undertaken on top of the trench and on the vertical trench wall is used in combination with a high-resolution digital elevation model (DEM) from t-LiDAR scanning. This allows radar facies (Neal, 2004) to be distinguished and the sedimentological architecture at depth within the trench wall to be identified. Thus, the resulting 3-D model from the GPR provides information on varying layer thicknesses and minimises misinterpretation due to cutting effects. The workflow comprising data acquisition, statistical analysis, interpretation and storage was calibrated on a road cut on the Island of Crete. We then applied this workflow on a professionally excavated trench in mainland Greece.

2 Geological setting of the study sites

The study sites are both located in Greece, which is one of the most seismically active parts of the Mediterranean (McKenzie, 1972; Le Pichon and Angelier, 1979; Papazachos et al., 2000) due to the presence of the Hellenic Arc and Trench System. Crustal extension orientated both arc-parallel and arc-perpendicular (Mariolakos and

An objective multiparametric interpretation of palaeoseismic trench stratigraphy

S. Schneiderwind et al.

Title Page

Abstract

Introduction

Conclusions

References

Tables

Figures

◀

▶

◀

▶

Back

Close

Full Screen / Esc

Printer-friendly Version

Interactive Discussion



Papanikolaou, 1981; Lyon-Caen et al., 1988) has led to the development of bedrock fault scarps throughout both mainland Greece (Stewart and Hancock, 1991; Benedetti et al., 2002) and the island of Crete (e.g. Wiatr et al., 2013). These normal faults mainly consist of footwall Mesozoic carbonates juxtaposed against hanging-wall flysch and/or post-alpine sediments. Earthquake features such as colluvial wedges (a consequence of degradation of the scarp), fissure fills and displaced strata occur within the hanging-walls of these faults and datable material may be contained within buried palaeosols (see Fig. 1vi) (McCalpin, 2009). To create those archives and preserve them over geological timescales, erosional processes must be lower than the rate of tectonic activity. These features therefore represent geological archives of palaeoearthquakes because they can record information about Holocene and Late Pleistocene earthquakes (e.g. Morey and Schuster, 1999; McCalpin, 2009). Ambraseys and Jackson (1990) estimate a maximum earthquake magnitude of M_s 7.0 could occur on these normal faults, which coincides with fault segment lengths of 15–30 km as determined through empirical relationships (Wells and Coppersmith, 1994).

2.1 The Sfaka Fault (NE Crete, Greece)

The island of Crete is the largest within the Greek territory and is directly adjacent to the subduction zone between Europe and Africa. The NNE–SSW trending Sfaka fault is located in northeastern Crete (Fig. 1i) and forms the easternmost segment within the Ierapetra Fault Zone which is a major tectonic line of approximately 25 km cutting through the whole island (Gaki-Papanastassiou et al., 2009). This northwest dipping normal fault is easy to recognise as it offsets smooth mountain slopes, has a steeply dipping (ca. 70°) fault scarp up to 6 m in height, and has an onshore length of approximately 5 km (Fig. 1iv). Together with the opposing Lastros fault a 2 km wide graben structure is formed.

An outcrop in the form of a road cut (located at 35°7′58.97″ N, 25°54′26.01″ E) exhibits the fault zone as a contact between footwall Mesozoic carbonates and hanging-

wall colluvium (Fig. 1v). The outcrop cuts the fault at an angle of approximately 75° from the fault strike.

2.2 The Kaparelli Fault (Gulf of Corinth, Greece)

The Kaparelli fault is located in the easternmost part of the Gulf of Corinth (see Fig. 1i) which is associated with rapid extension oriented N-S (e.g. Papanikolaou and Royden, 2007). The Kaparelli fault became well-known as it ruptured during the Corinthian Alkyonides earthquake sequence in spring 1981 (Jackson et al., 1982). Many palaeoseismological studies using various approaches have been undertaken along this ca. 20 km long south dipping normal fault. For example Benedetti et al. (2003) used ^{36}Cl cosmic ray exposure dating to determine the history of surface rupturing events on the 4–5 m high limestone scarp of the Kaparelli fault. Their results show evidence for seismic activity 20 ± 3 , 14.5 ± 0.5 and 10.5 ± 0.5 ka prior to the 1981 earthquake sequence. A palaeoseismological trenching study was conducted by Kokkalas et al. (2007). The authors found evidence for at least three events in the past 10 000 years: 9370 ± 120 , 7290 ± 140 and 1165 ± 105 a. The excavations from Kokkalas et al. (2007) are still open; therefore, the already logged and interpreted structures within trench Kap-1 (Fig. 1v) is a perfect site to test the workflow developed on the Sfaka fault road cut.

3 Methodology

The herein presented workflow combines palaeoseismic trenching techniques with t-LiDAR measurements to improve the accuracy of palaeoearthquake reconstruction. A multispectral analysis of t-LiDAR backscatter data and the luminescence of true colour photographs were compared to the manual trench log. A GPR survey was then conducted to obtain 3-D information of layer continuation and thickness in depth within the trench wall (Fig. 2).

SED

7, 2697–2733, 2015

An objective multiparametric interpretation of palaeoseismic trench stratigraphy

S. Schneiderwind et al.

Title Page

Abstract

Introduction

Conclusions

References

Tables

Figures

◀

▶

◀

▶

Back

Close

Full Screen / Esc

Printer-friendly Version

Interactive Discussion



3.1 Palaeoseismic trenching

A palaeoseismic trench is characterised by an often artificially produced subsurface exposure of sedimentological coseismic features. To accurately interpret these features, apparent dips and anthropogenic and/or exogenous influences must be excluded.

Moreover, sketching lithological contents requires an exposure devoid of weathered and smeared parts that were caused by the excavation (McCalpin, 2009). To simplify and prove the geometrical correctness of the trench log, a reference grid of one square metre was attached to the wall. The grid's points of intersection also act as reference points for remote sensing applications.

The trenches were conventionally logged in 1 : 10 scale in accordance with McCalpin (2009). Thereby, discrete deposits that are composed of similar lithology considering consistent texture, sorting, bedding, fabric, and colour of individual layers are mapped. Photographs of every square metre were taken and later stitched together using an automatic panorama recognising tool including a manual editor of control points and straightening functions (Autopano Giga, Kolor). It must be noted that error values are already stored within image information due to differing luminous exposures; furthermore, holes and protruding boulders create shadows that partially change the reflection characteristics of certain sedimentological features. The Sfaka road cut faces north (see Fig. 1iv and v) and is surrounded by steep slopes. In Kaparelli the eastern trench wall (see Fig. 1ii and iii) was investigated because it preserved the best stratigraphy and exhibits faulting events with clear marker horizon displacements (Kokkalas et al., 2007). To avoid most of the differing luminous exposures, the photographs were either taken in the morning when the angle of sunlight was shallow and did not shine directly onto the investigated wall (Kaparelli) or in the afternoon when the sun disappeared behind the surrounding hills (Sfaka).

The photomosaic of true colour images (RGB; red, green, blue) was converted into a grey-level image to eliminate hue and saturation information while retaining the luminance (0–255) using the `rgb2gray` function in MATLAB[®]. In a GIS the resulting im-

An objective multiparametric interpretation of palaeoseismic trench stratigraphy

S. Schneiderwind et al.

Title Page

Abstract

Introduction

Conclusions

References

Tables

Figures

◀

▶

◀

▶

Back

Close

Full Screen / Esc

Printer-friendly Version

Interactive Discussion



age was georeferenced to a custom frame in order to make it comparable to all other datasets of this study.

3.2 t-LiDAR measurements

t-LiDAR (terrestrial Light Detection and Ranging) is a remote sensing technique with high spatial and temporal resolution and is a very effective instrument for reconstructing morphological and geological settings and monitoring approaches. A generated coherent laser beam with little divergence by stimulated emission is reflected off surfaces and the proportionate backscattered signal is detected, forming a non-contact and non-penetrative active and stationary recording system. Thus, from measuring the two-way-travel time (TWT) of a first pulse detection sequence, 3-D surface data is acquired. The illuminated area is controlled by wavelength, beam divergence, range between sensor and target, and also by the angle of incidence (Jörg et al., 2006; Wiatr et al., 2015). In our study we used an ILRIS 3-D laser ranging system (wavelength λ is 1500 nm) from OPTECH Inc., Ontario, Canada.

The limitations of using t-LiDAR are high humidity (e.g. Lobell and Asner, 2002) and low target reflection with cumulative distance and shallow incident angle (e.g. Höfle and Pfeifer, 2007). In order to assume constant soil moisture and to ensure the backscatter signal data quality, close range scans were done during the summer in dry conditions within a few hours. The scans were carried out almost perpendicular to the trench wall and less than 10 m from the exposure.

Other benefits of applying t-LiDAR is its flexibility, the relatively quick availability of an actual dataset, and also its high spatial resolution with information about backscatter signal each referenced in x , y , z coordinates. The result is an irregular but dense point cloud representing a highly detailed digital 3-D surface model which can be easily implemented in geographical information systems (GIS) to generate accurate digital elevation models (DEM) or digital terrain models (DTM) (e.g. Wiatr et al., 2015).

For this study, the t-LiDAR scanning was undertaken at both close range and long-mid range to determine geometrical relationships between the footwall, hanging-wall,

An objective multiparametric interpretation of palaeoseismic trench stratigraphy

S. Schneiderwind et al.

Title Page

Abstract

Introduction

Conclusions

References

Tables

Figures

◀

▶

◀

▶

Back

Close

Full Screen / Esc

Printer-friendly Version

Interactive Discussion



An objective multiparametric interpretation of palaeoseismic trench stratigraphy

S. Schneiderwind et al.

Title Page

Abstract

Introduction

Conclusions

References

Tables

Figures

◀

▶

◀

▶

Back

Close

Full Screen / Esc

Printer-friendly Version

Interactive Discussion



De Rose et al., 2011; Nouri et al., 2014). Ragona et al. (2006) introduced an application of high-resolution field imaging spectroscopy on paleoseismic exposures using hyperspectral and common digital photo cameras. The authors conclude that imaging spectroscopy can be successfully applied to assist in the description and interpretation of palaeoseismic exposures because: (i) subtle or invisible features are displayed, (ii) quantitative analysis and comparisons of units using reflectance spectra can be undertaken, and (iii) unbiased data are stored for future access and analysis.

The limitations of multispectral approaches are, by their very nature, closely connected to the application of photomosaics and t-LiDAR measurements. We re-emphasise the influence of moisture; where present it not only causes a darkening of the sediments (reduction in reflectance), but there is also a hard-to-quantify content variation across the exposure (Ragona et al., 2006). Another error source appears due to morphological characteristics of a certain exposure, especially on surfaces that are not well prepared for palaeoseismic investigations and data collection. This means that the exposure must be flattened and cleaned to avoid changes in spectral amplitudes accompanying changes in illumination angle and distance.

To reduce errors we assume that the moisture content was similar throughout the exposure and water absorptions should not affect the correlations because the spectral change is similar along the trench wall. Furthermore, the photos and t-LiDAR scans were taken almost perpendicular to the exposure so that optimal data quality can be expected.

The workflow contains geo-referencing and snapping the high-resolution raster data from the photomosaic and t-LiDAR backscatter signal to a coherent cell size (0.001 m) in a GIS. Afterwards, an iso (iterative self-organising) cluster unsupervised classification was applied to a two-channel composition of both raster layers. Thereby, the number of classes was set to ten times the amount of included bands (photomosaic grey-level image and t-LiDAR backscatter signal image) as this provides sufficient statistics and enough cells to accurately represent a certain cluster. This type of clustering uses a process in which all samples are assigned to existing cluster centres during each iter-

ation; new means are then recalculated for every class. The actual number of classes is usually unknown; therefore, we started with 20 classes and analysed the attribute distances between sequentially merged classes with the dendrogram method (hierarchical clustering). This reduces statistical misclassifications and provides information on distinct classes. Based on the outcome, classes which are statistically closest get merged and the dataset gets reclassified. Block statistics within a 3 × 3 cell environment are applied to erase noise by overwriting cell values to all of the cells in each block with the median value (Fig. 3). Moreover, resampling down to 0.02 m cells enhances visibility and allows a more general interpretation and comparison to the conventional log. This is because average gridding and sketching inaccuracy is around 2 % (McCalpin, 2009).

3.4 Ground-penetrating radar

GPR is a non-invasive and non-destructive geophysical technique that operates with high-frequency electromagnetic waves in the radio band to detect electrical discontinuities in the shallow subsurface up to approximately 50 m. Every GPR measurement contains a five-step process: (i) generating, (ii) transmitting, (iii) propagating, (iv) reflecting, and (v) receiving electromagnetic pulses. The differing relative dielectric permittivities (ϵ_r) of varying materials control the transmitting velocity in relation to the speed of light ($c = 0.2998 \text{ m ns}^{-1}$) once the pulse is emitted from the antenna. Fractional reflections of the pulse on inhomogeneities and layer boundaries get received due to a dielectric contrast. In order to calculate depths of reflection the TWT (two way travel-time) is recorded in the order of nanoseconds. Depending on the frequency of the antenna, objects smaller than 0.1 m in diameter can be resolved. Common GPR systems perform at frequencies between 50 MHz and 1 GHz, where achievable resolution is a quarter of the wavelength. The relationship between penetration depth and spatial resolution is an inverse one; hence, a higher spatial resolution occurs at the expense of penetration depth and vice versa (Neal, 2004; Schrott and Sass, 2008).

An objective multiparametric interpretation of palaeoseismic trench stratigraphy

S. Schneiderwind et al.

Title Page

Abstract

Introduction

Conclusions

References

Tables

Figures

◀

▶

◀

▶

Back

Close

Full Screen / Esc

Printer-friendly Version

Interactive Discussion



An objective multiparametric interpretation of palaeoseismic trench stratigraphy

S. Schneiderwind et al.

Title Page

Abstract

Introduction

Conclusions

References

Tables

Figures

◀

▶

◀

▶

Back

Close

Full Screen / Esc

Printer-friendly Version

Interactive Discussion



Water is almost the only limiting parameter for the application of GPR because of its high relative dielectric permittivity. Moisture content dramatically decreases the electromagnetic wave velocity by stronger attenuation and leads to reduced penetration depths (Schrott and Sass, 2008). Soil moisture differences often severely disrupt wave energy, which makes it even more difficult to interpret reflections. Dielectric contrasts are the main features of the GPR image interpretation, since any dielectric discontinuity is detected. Thus, targets can be classified according to their geometry and reflection facies.

GPR was carried out on the vertical trench wall and on the slope surface above the trench (see Fig. 2). In order to make the GPR operationally effective, our survey provided efficient coupling of electromagnetic radiation into the ground and a sufficiently large scattered signal for detection at or above the ground surface. Furthermore, a 400 MHz antenna together with a SIR-3000 control unit from Geophysical Survey Systems Inc. (GSSI, Salem, NH, USA) was used to obtain desired resolution and noise levels. The data processing was done using the software ReflexW[®] (Sandmeier Scientific Software, Karlsruhe, Germany) involving the following processing sequence: remove header gain, move start time, energy decay, 1-D bandpass frequency, background removal, and average xy . Reflection hyperbolas of gravels were used to estimate wave velocity. Data migration was undertaken to correct angles, because dips are usually underestimated due to a complex 3-D cone in which electromagnetic energy radiates (Neal, 2004).

Based on distinct layers in the trench log and taking into account the results of the multispectral analysis, GPR-data were then used to interpret the outcropping strata in 3-D.

4 Results

4.1 Sfaka Fault, Crete

4.1.1 Trench log

In accordance with McCalpin (2009) the trench was logged and divided into ten distinct layers. These vary in colour, matrix specifications, geometrical alignments and soil formation. As seen in Fig. 4a, two palaeosols that depict fissure fills are observed in the trench wall. These layers represent hanging-wall sediments, rather than material from the footwall. Overlying deposits rapidly filled ground cracks that occur during a rupturing event. Both palaeosols contain a combination of fine-grained and gravel sized material. Colluvial layers of gravels of different colour and component size and orientation complete the hanging wall's architecture to its western end (see Fig. 4a, C1–C6). However, C1 is made of heavily cemented colluvial material and thus will not be further addressed. Adjacent to the bedrock fault plane towards the eastern end of the trench wall, fault gouge of approximately 1 m thickness is exposed. However, true thickness is calculated to around 0.8 m when correcting for the trench's 75° from fault strike. The yellowish light coloured fine-grained cohesive matrix obviously differs from other sediments within the hanging wall exposure (Fig. 4b).

4.1.2 Imaging spectroscopy

The greyscale photomosaic stores visual impressions in a way similar to the human eye and represents a weighted sum value of luminance within the range of visible light per pixel. Luminance at 1500 nm detected by t-LiDAR significantly differs in some parts of the trench wall (Fig. 4b and c). As shown in Table 1, the light fault gouge material is highly reflective in both photomosaic and HRDBSM.

The homogeneous silty layer contains only a view voids due to excavation works that influence reflectance value range. Resultant colorimetric shift expressed by the 2-

SED

7, 2697–2733, 2015

An objective multiparametric interpretation of palaeoseismic trench stratigraphy

S. Schneiderwind et al.

Title Page

Abstract

Introduction

Conclusions

References

Tables

Figures

◀

▶

◀

▶

Back

Close

Full Screen / Esc

Printer-friendly Version

Interactive Discussion



An objective multiparametric interpretation of palaeoseismic trench stratigraphy

S. Schneiderwind et al.

Title Page

Abstract

Introduction

Conclusions

References

Tables

Figures

◀

▶

◀

▶

Back

Close

Full Screen / Esc

Printer-friendly Version

Interactive Discussion

component composition almost solely depicts the highest value ranges for this part of the trench wall (Fig. 4d). In contrast, the cemented colluvium to the west is highly irregular in the sense of reflectance. Both photomosaic and HRDBSM show a heterogeneous greyscale value distribution that is even more embodied by high-grade contrasts in the two-channel composition. Similar observations occur for larger boulders that protrude out of the trench wall (Fig. 4a–d).

Colluvial layers C2–C5 are distinctively different in their reflectance characteristics. Where transition between both units is indeed visible in the photomosaic, a sharp contrast in reflectance characteristics of near-infrared is recognisable. Moreover, the named colluvial deposits do not only appear as a conglomerate of diffuse values but show evidence of alignments. An upward oriented structure of approximately 0.5 m thickness is obvious in HRDBSM and false colour composition. The structure follows a lineament of displacement within the colluvial strata.

Figure 5 visualises percentages of seven classes, estimated from the unsupervised classification on individual identified layers within the trench log. Either the majority of a certain layer is fulfilled by one single class or by a certain composition of two or three classes. Where Table 1 shows the dominance of high values within the fault gouge layer, the illustration of unsupervised classification proves this layer to be almost completely (70 %) represented by one single class (7). Although class 4 covers almost the same value range as class 7, fault gouge exposure is only covered by 8 % by class 4 (see Fig. 5a).

In the unsupervised classification, the fault gouge is the only layer in this trench wall where the majority is covered by one single class. Palaeosol I and palaeosol II have a similar ratio of effecting classes but class 6 is not present in the palaeosol II signature, allowing them to be differentiated. By visualising the spatial arrangement of influencing classes the differentiation between these two layers is even better (Fig. 4e). While Fig. 5b only shows percentage significance of class ratios per layer, the spatial distribution promotes the reconstruction of a certain layer. The accumulation of class 5

especially in the lower part of palaeosol I is obviously different from any other cluster in palaeosol II, although quantitative statistics conclude a similar composition of classes.

Except for C6, which is well represented to around 80% by class 1 (31%) and 2 (52%), and C1, which appears as a unsorted conglomerate of classified responses, the remaining colluvial lithologies appear with similar ratios, especially classes 1, 2, and 5. In a quantitative way no distinction can be recognised. Also, large scale clustering of classes within the layers is absent. However, arrangements, especially of class 7, are obvious and coincide with coarse-grained gravels within the colluvium. Within C3 a micro-cluster of approximately 25 pixels are arranged along a slightly bent line dipping about 50° towards the footwall. A similar arrangement of class 7 with an even smaller cluster (3 × 3 pixels) and wider spread is indicated in C5 dipping 15° towards the footwall. Furthermore, the surrounding matrix is slightly more expressed by class 5 in C5, whereas C3 has subjectively no preferred matrix content (Fig. 4). Alterations are expected to decrease with increasing depth. Dependent on rock composition and mean annual precipitation, the formation of new minerals is commonly related to depth from surface. C4 does not show any spectroscopical attribute except for a complete absence of class 6 and low range greyscale values (see Fig. 5a). Clasts or large boulders protruding out of the trench wall are represented by intermediate value range class 5 on top and wide value range class 1 at the bottom (Fig. 4c).

4.1.3 GPR

Using the trench log and multispectral information enables radar facies to be distinguished. Figure 6 confirms the distinction of individual layers by comparison of reflected electromagnetic signal intensity. Reflections of visible and near-infrared light within certain zones that fit with trace increment and dimensions of the GPR system (30 cm × 2 cm) were sampled and correlated with the radar's first arrival. As the vertical resolution is a quarter of the wavelength λ (here: 30–40 cm), we averaged reflection amplitudes for 9 cm into depth per trace.

An objective multiparametric interpretation of palaeoseismic trench stratigraphy

S. Schneiderwind et al.

Title Page

Abstract

Introduction

Conclusions

References

Tables

Figures

◀

▶

◀

▶

Back

Close

Full Screen / Esc

Printer-friendly Version

Interactive Discussion



An objective multiparametric interpretation of palaeoseismic trench stratigraphy

S. Schneiderwind et al.

Title Page

Abstract

Introduction

Conclusions

References

Tables

Figures

◀

▶

◀

▶

Back

Close

Full Screen / Esc

Printer-friendly Version

Interactive Discussion

A good correlation between backscattered signals of both passive and active methods is obvious in some parts. A significant contrast in all three datasets is traced by the abrupt transition from fault gouge to palaeosol I (see Figs. 4c and 6). Where reflections of visible and near-infrared light are intense on the surface of the fault gouge exposure, they rapidly decrease in signal strength on the palaeosol surface. The opposite reflectance behaviour is observed for radar reflections in the very shallow subsurface; the first lithological transition is characterised by the change of low to moderate reflection amplitudes in the fine-grained homogeneous fault gouge to higher reflection intensities from heterogeneous palaeosol I.

Moderate reflectance with intermediate variance designates the exposure of palaeosol I. A slightly decreasing trend is obvious within this section just before an abrupt rise in both visible and near-infrared light reflection values. This changeover is not obvious from GPR mean values. However, value range given by standard deviation reach wider than the in previous section. Moreover, there is little distinction between individual colluvial deposits from GPR reflection amplitudes.

As previously stated, the HRDBSM shows an unrecognised feature in the middle of the trench exposure. A change is proven by a drastic drop in reflections from the GPR signal approximately 3 m from the fault plane. At the same position there is also a minor photomosaic and HRDBSM value decline. Thus, a conspicuous progression similar to a Gaussian bell shape curve in the middle of a dataset is obvious.

Layer C1 is not individually considered since the coupling of the antenna on heavily weathered cemented material with rugged surface relief was not sufficient. However, other transitions recognised in trench log and imaging spectroscopy can be traced in GPR images. This then leads to a 3-D model of coseismic features within the hanging-wall (Fig. 7). Seven out of the ten (boulders are not included as an individual layer) previously mapped units plus the limestone fault plane to the West and the adjacent loose material to the East can be traced at depth using GPR.

The 3-D interpretation from GPR images visualises the continuation of distinct layers observed from multispectral analysis into depth. The limestone fault plane and fault

a multispectral view of the palaeoseismic exposure, which allows quantitative information to be assigned to mapped units within the trench wall.

There are some significant disadvantages of passive data collection imaging techniques. These are mainly due to differing angles of illumination because the trench exposure is not a perfectly even surface at all scales; at larger scales surface undulations dramatically increase. Thus, the lightest parts in the photomosaic, visualised for the Sfaka roadcut as class 7 with an average value of 221, mainly represent a high matrix luminance and the top (bright) sides of boulders and clasts. Rectification and parallax effects yield an additional error in the order of a few centimetres. High-resolution 3-D images and the near infrared backscatter signal from t-LiDAR provide information on the physical properties of materials. Colour, matrix specifications, geometrical alignments and soil formation features influence the t-LiDAR backscatter signal. A multispectral approach, using unsupervised clustering on both spectra supports the results from the trench log and complements the findings. Thereby, a distinct layer signature given by particular compositions of effecting classes allows adjacent stratigraphic units to be differentiated. Some areas within the multispectral image lack evidence for distinct spectroscopical characteristics. However, these areas can still be defined when they are adjacent to areas with static characteristics; the boundary between two areas is clearly defined as long as one area can be classified using the unsupervised clustering. Therefore, a spectroscopically inconspicuous and completely heterogeneous area surrounded by regions with static characteristics is still sufficiently confined. Within a given error range due to manual gridding on the trench wall, georectification and blending pixels of the photomosaic data, the results show many resemblances to the manually drawn trench log.

The results of the imaging spectroscopy verified the lithology of the trench wall and the resulting image from the unsupervised classification serves as a calibration factor for GPR measurements. Due to the GPR's resolution being about 0.1 m, the calibration is necessary to recognise and interpret minor differences in sedimentological compositions. This method allows more accurate calculations of geometric layer thicknesses to

SED

7, 2697–2733, 2015

An objective multiparametric interpretation of palaeoseismic trench stratigraphy

S. Schneiderwind et al.

Title Page

Abstract

Introduction

Conclusions

References

Tables

Figures

◀

▶

◀

▶

Back

Close

Full Screen / Esc

Printer-friendly Version

Interactive Discussion

An objective multiparametric interpretation of palaeoseismic trench stratigraphy

S. Schneiderwind et al.

Title Page

Abstract

Introduction

Conclusions

References

Tables

Figures

◀

▶

◀

▶

Back

Close

Full Screen / Esc

Printer-friendly Version

Interactive Discussion



the experience of the trench logger, and is thus subjectively influenced. Hence, (minor) differences in lithological description from expert to expert are expected, especially if one logger has access to no more than a photomosaic. In order to prove whether conventional trench logging methods used to map coseismic features in a palaeoseismic trench wall can be objectively enhanced, we created an accurate digital version of the exposure and its physical properties. This was done by combining routine logging with vertical GPR measurements and imaging spectroscopic approaches from normalised photomosaics and high resolution t-LiDAR backscatter models. Both the studied palaeoseismic exposures, on Crete and in mainland Greece, exhibit sedimentary structures whose constituent parts and shape are essential information for a palaeoseismic reconstruction.

After the conventional trench logging was completed, t-LiDAR scans were undertaken at close range. The near-infrared backscattered signal was combined with a luminance bearing photomosaic of the same trench wall. Statistical and classification techniques reproduce an objective digital copy of a palaeoseismic trench log. In order to define distinct units, four options to characterise and differentiate individual layers by imaging spectroscopy can be registered:

- Significant dominance of a certain class within a distinct layer.
- Certain composition with spatial clustering.
- Certain composition with certain arrangements.
- Distinct borders between individual layers although one or both are not determined by applied statistics.

Subtle or invisible features are enhanced and become part of a quantitative analysis, and comparisons of units using their reflectance on certain wavelengths (see also Ragona et al., 2006) can be carried out. Our results show that based on distinct layers in the trench log, in combination with the outcome of imaging spectroscopy, a 3-D-interpretation of GPR-data carried out vertically on the trench wall is possible. Hence,

An objective multiparametric interpretation of palaeoseismic trench stratigraphy

S. Schneiderwind et al.

Title Page

Abstract

Introduction

Conclusions

References

Tables

Figures

◀

▶

◀

▶

Back

Close

Full Screen / Esc

Printer-friendly Version

Interactive Discussion



Bubeck, A., Wilkinson, M., Roberts, G. P., Cowie, P. A., McCaffrey, K., Phillips, R., and Sammonds, P.: The tectonic geomorphology of bedrock scarps on active normal faults in the Italian Apennines mapped using combined ground penetrating radar and terrestrial laser scanning, *Geomorphology*, 237, 38–51, 2015.

5 Bull, W. B.: *Tectonic Geomorphology of Mountains: a New Approach to Paleoseismology*, Blackwell Pub., Malden, MA, 316 pp., 2007.

Carcaillet, J., Manighetti, I., Chauvel, C., Schlagenhauf, A., and Nicole, J.-M.: Identifying past earthquakes on an active normal fault (Magnola, Italy) from the chemical analysis of its exhumed carbonate fault plane, *Earth Planet. Sc. Lett.*, 271, 145–158, 2008.

10 Chow, J., Angelier, J., Hua, J.-J., Lee, J.-C., and Sun, R.: Paleoseismic event and active faulting: from ground penetrating radar and high-resolution seismic reflection profiles across the Chihshang Fault, eastern Taiwan, *Tectonophysics*, 333, 241–259, 2001.

Demagnet, D., Renardy, F., Vanneste, K., Jongmans, D., Camelbeeck, T., and Meghraoui, M.: The use of geophysical prospecting for imaging active faults in the Roer Graben, Belgium, *Geophysics*, 66, 78–89, 2001.

15 De Rose, R. C., Oguchi, T., Morishima, W., and Collado, M.: Land cover change on Mt. Pinatubo, the Philippines, monitored using ASTER VNIR, *Int. J. Remote Sens.*, 32, 9279–9305, 2011.

Gaki-Papanastassiou, K., Karymbalis, E., Papanastassiou, D., and Maroukian, H.: Quaternary marine terraces as indicators of neotectonic activity of the Ierapetra normal fault SE Crete (Greece), *Geomorphology*, 104, 38–46, 2009.

20 Grützner, C., Reicherter, K., Hübscher, C., and Silva, P. G.: Active faulting and neotectonics in the Baelo Claudia area, Campo de Gibraltar (southern Spain), *Tectonophysics*, 554–557, 127–142, 2012.

25 Grützner, C., Barba, S., Papanikolaou, I. D., and Pérez-López, R.: Earthquake geology: science, society and critical facilities, *Ann. Geophys.-Italy*, 56, S0683, doi:10.4401/ag-6503, 2013.

Höfle, B. and Pfeifer, N.: Correction of laser scanning intensity data: data and model-driven approaches, *ISPRS J. Photogramm.*, 62, 415–433, 2007.

30 Jackson, J. A., Gagnepain, J., Houseman, G., King, G., Papadimitriou, P., Soufleris, C., and Virieux, J.: Seismicity, normal faulting, and the geomorphological development of the Gulf of Corinth (Greece): the Corinth earthquakes of February and March 1981, *Earth Planet. Sc. Lett.*, 57, 377–397, 1982.

An objective multiparametric interpretation of palaeoseismic trench stratigraphy

S. Schneiderwind et al.

Title Page

Abstract

Introduction

Conclusions

References

Tables

Figures

◀

▶

◀

▶

Back

Close

Full Screen / Esc

Printer-friendly Version

Interactive Discussion



Jörg, P., Fromm, R., Sailer, R., and Schaffhauser, A.: Measuring snow depth with a terrestrial laser ranging system, International Snow Science Workshop, 1–6 October 2006, Telluride, CO, USA, 452–460, 2006.

Keller, E. A. and Rockwell, T. K.: Tectonic Geomorphology, Quaternary chronology, and Paleoseismicity, in: Tectonic Geomorphology, Quaternary Chronology, and Paleoseismicity, Developments and Applications of Geomorphology, edited by: Costa, J. E. and Fleisher, P. J., Springer, Berlin, Heidelberg, 203–239, 1984.

Kokkalas, S. and Koukouvelas, I. K.: Fault-scarp degradation modeling in central Greece: the Kaparelli and Eliki faults (Gulf of Corinth) as a case study, *J. Geodyn.*, 40, 200–215, 2005.

Kokkalas, S., Pavlides, S., Koukouvelas, I. K., Ganas, A., and Stamatopoulos, L.: Paleoseismicity of the Kaparelli fault (eastern Corinth Gulf): evidence for earthquake recurrence and fault behaviour, *Boll. Soc. Geol. Ital.*, 126, 387–395, 2007.

Le Pichon, X. and Angelier, J.: The hellenic arc and trench system: a key to the neotectonic evolution of the eastern mediterranean area, *Tectonophysics*, 60, 1–42, 1979.

Lobell, D. B. and Asner, G. P.: Moisture effects on soil reflectance, *Soil Sci. Soc. Am. J.*, 66, 722–727, doi:10.2136/sssaj2002.7220, 2002.

Lyon-Caen, H., Armijo, R., Drakopoulos, J., Baskoutass, J., Delibassis, N., Gaulon, R., Kouskouna, V., Latoussakis, J., Makropoulos, K., Papadimitriou, P., Papanastassiou, D., and Pedotti, G.: The 1986 Kalamata (South Peloponnesus) Earthquake: detailed study of a normal fault, evidences for east–west extension in the Hellenic Arc, *J. Geophys. Res.*, 93, 14967, doi:10.1029/JB093iB12p14967, 1988.

Machette, M. N.: Active, capable, and potentially active faults – a paleoseismic perspective, *J. Geodyn.*, 29, 387–392, 2000.

Mariolakos, I. and Papanikolaou, D. J.: The Neogene basins of the Aegean Arc from the Paleogeographic and the Geodynamic point of view, in: Proc. Int. Symp. H. E. A. T., Athens, Greece, 8–10 April 1981, 383–399, 1981.

McCalpin, J.: Paleoseismology, 2nd edn., International Geophysics Series, v. 95, Academic Press, Burlington, MA, 613 pp., 2009.

McKenzie, D.: Active tectonics of the Mediterranean region, *Geophys. J. Roy. Astr. S.*, 30, 109–185, 1972.

Michetti, A. M., Audemard, M., Franck, A., and Marco, S.: Future trends in paleoseismology: integrated study of the seismic landscape as a vital tool in seismic hazard analyses, *Tectonophysics*, 408, 3–21, 2005.

An objective multiparametric interpretation of palaeoseismic trench stratigraphy

S. Schneiderwind et al.

Title Page

Abstract

Introduction

Conclusions

References

Tables

Figures

◀

▶

◀

▶

Back

Close

Full Screen / Esc

Printer-friendly Version

Interactive Discussion

- Morey, D. and Schuster, G. T.: Palaeoseismicity of the Oquirrh Fault, Utah from shallow seismic tomography, *Geophys. J. Int.*, 138, 25–35, 1999.
- Neal, A.: Ground-penetrating radar and its use in sedimentology: principles, problems and progress, *Earth-Sci. Rev.*, 66, 261–330, 2004.
- 5 Nouri, H., Beecham, S., Anderson, S., and Nagler, P.: High Spatial Resolution WorldView-2 Imagery for Mapping NDVI and its relationship to temporal urban landscape evapotranspiration factors, *Remote Sensing*, 6, 580–602, 2014.
- Papanikolaou, D. J. and Royden, L. H.: Disruption of the Hellenic arc: late Miocene extensional detachment faults and steep Pliocene-Quaternary normal faults – or what happened at Corinth?, *Tectonics*, 26, TTC5003, doi:10.1029/2006TC002007, 2007.
- 10 Papanikolaou, I. D., van Balen, R., Silva, P. G., and Reicherter, K.: Geomorphology of active faulting and seismic hazard assessment: new tools and future challenges, *Geomorphology*, 237, 1–13, 2015.
- Papazachos, B. C., Comnakis, P. E., Karakaisis, G. F., Karakostas, B. G., Papaioannou, C., Papazachos, C. B., and Scordilis, E. M.: A Catalogue of Earthquakes in Greece and Surrounding Area for the Period 550 BC–1999, *Publ. Geophys. Laboratory, University of Thessaloniki, Thessaloniki, Greece*, 1, 333 pp., 2000.
- 15 Ragona, D., Minster, B., Rockwell, T., and Jussila, J.: Field imaging spectroscopy: a new methodology to assist the description, interpretation, and archiving of paleoseismological information from faulted exposures, *J. Geophys. Res.*, 111, B10309, doi:10.1029/2006JB004267, 2006.
- Reicherter, K.: Paleoseismologic advances in the Granada Basin (Betic Cordilleras, southern Spain), *Paleoseismology of Spain, Acta Geologica Hispanica, Barcelona, Special Volumes*, 36, 267–281, 2001.
- 25 Reicherter, K., Jabaloy, A., Galindo-Zaldívar, J., Ruano, P., Becker-Heidmann, P., Morales, J., Reiss, S., and González-Lodeiro, F.: Repeated palaeoseismic activity of the Ventas de Zafaraya fault (S Spain) and its relation with the 1884 Andalusian earthquake, *Int. J. Earth Sci.*, 92, 912–922, 2003.
- Reicherter, K., Michetti, A. M., and Barroso, P. G. S.: Palaeoseismology: historical and pre-historical records of earthquake ground effects for seismic hazard assessment, *Geological Society, London, Special Publications*, 316, 1–10, 2009.
- 30

An objective multiparametric interpretation of palaeoseismic trench stratigraphy

S. Schneiderwind et al.

Title Page

Abstract

Introduction

Conclusions

References

Tables

Figures

◀

▶

◀

▶

Back

Close

Full Screen / Esc

Printer-friendly Version

Interactive Discussion



Reiss, S., Reicherter, K., and Reuther, C.-D.: Visualization and characterization of active normal faults and associated sediments by high-resolution GPR, Geological Society, London, Special Publications, 211, 247–255, 2003.

Sabins, F. F.: Remote Sensing: Principles and Interpretation, 3rd edn., edited by: Freeman, W. H. and Co., W. H. Freeman Electronic Publishing Center/Andrew Kudlacik, New York, USA, 494 pp., 1997.

Schrott, L. and Sass, O.: Application of field geophysics in geomorphology: advances and limitations exemplified by case studies, *Geomorphology*, 93, 55–73, 2008.

Sieh, K. E.: Prehistoric large earthquakes produced by slip on the San Andreas Fault at Pallett Creek, California, *J. Geophys. Res.*, 83, 3907, doi:10.1029/JB083iB08p03907, 1978.

Stewart, I. and Hancock, P.: Scales of structural heterogeneity within neotectonic normal fault zones in the Aegean region, *J. Struct. Geol.*, 13, 191–204, 1991.

Tucker, C. J.: Red and photographic infrared linear combinations for monitoring vegetation, *Remote Sens. Environ.*, 8, 127–150, 1979.

Wallace, R. E.: Active Tectonics: Impact on Society, The National Academies Press, Washington, DC, 1986.

Wells, D. L. and Coppersmith, K. J.: New empirical relationships among magnitude, rupture length, rupture width, rupture area, and surface displacement, *B. Seismol. Soc. Am.*, 84, 974–1002, 1994.

Wesnousky, S. G.: Earthquakes, quaternary faults, and seismic hazard in California, *J. Geophys. Res.*, 91, 12587–12631, 1986.

Wiatr, T., Reicherter, K., Papanikolaou, I., Fernández-Steeger, T., and Mason, J.: Slip vector analysis with high resolution t-LiDAR scanning, *Tectonophysics*, 608, 947–957, 2013.

Wiatr, T., Papanikolaou, I., Fernández-Steeger, T., and Reicherter, K.: Bedrock fault scarp history: insight from t-LiDAR backscatter behaviour and analysis of structure changes, *Geomorphology*, 228, 421–431, 2015.

Yeats, R. S. and Prentice, C. S.: Introduction to special section: paleoseismology, *J. Geophys. Res.*, 101, 5847–5853, doi:10.1029/95JB03134, 1996.

An objective multiparametric interpretation of palaeoseismic trench stratigraphy

S. Schneiderwind et al.

Table 1. Median greyscale values of photomosaic, high-resolution digital backscatter model (HRDBSM) and 2-component composition per stratigraphic unit from the trench log. The composition is the result of allocation of both, photomosaic and HRDBSM in equal parts, to visualise certainties and their variation within given zones. Error is given by single standard deviation.

Layer	Photomosaic	HRDBSM	Composition
recent topsoil	132 ± 21	197 ± 12	138 ± 23
fault gouge	221 ± 19	239 ± 12	224 ± 23
palaeosol I	165 ± 19	170 ± 13	87 ± 23
palaeosol II	156 ± 19	192 ± 10	128 ± 21
C6	131 ± 19	178 ± 10	99 ± 21
C5	152 ± 21	199 ± 11	142 ± 21
C4	143 ± 22	198 ± 10	140 ± 21
C3	171 ± 19	200 ± 12	144 ± 24
C2	147 ± 22	186 ± 13	116 ± 25
C1	144 ± 18	199 ± 15	144 ± 30
Boulder	168 ± 26	177 ± 15	102 ± 26

Title Page

Abstract

Introduction

Conclusions

References

Tables

Figures

◀

▶

◀

▶

Back

Close

Full Screen / Esc

Printer-friendly Version

Interactive Discussion

An objective multiparametric interpretation of palaeoseismic trench stratigraphy

S. Schneiderwind et al.

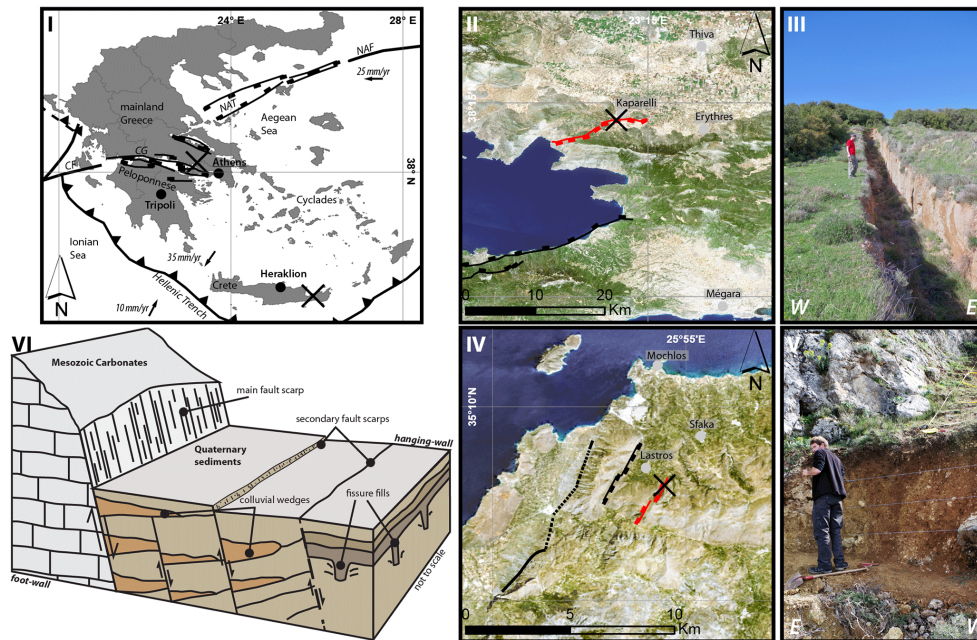


Figure 1. Guide to the study area. **(i)** Map of Greece showing simplified large-scale tectonic structures (CG, Corinthian Gulf; CF, Cephalonia fault; NAF, North Anatolian fault; NAT, North Anatolian Trough; black lines with barbs show active thrusts; black lines with marks show active faults) (after Kokkalas and Koukouvelas, 2005; Papanikolaou and Royden, 2007). Black crosses highlight study areas. **(ii)** Satellite image (Landsat 8, 2015) of the easternmost Gulf of Corinth. The Kaparelli fault is shown in red and the cross marks the position of the paleoseismological trench of Kokkalas et al. (2007). **(iii)** View of the Kaparelli trench. **(iv)** Satellite image (Landsat 8, 2015) of the study area at the Sfaka fault (red) in northeastern Crete; the cross shows the position of the road cut along strike. **(v)** View of the Sfaka road cut. **(vi)** Sketch of a typical post-glacial normal fault showing bedrock juxtaposed against Quaternary sediments which contain structures caused by recurrent earthquakes (modified after Reicherter et al., 2003).

An objective multiparametric interpretation of palaeoseismic trench stratigraphy

S. Schneiderwind et al.

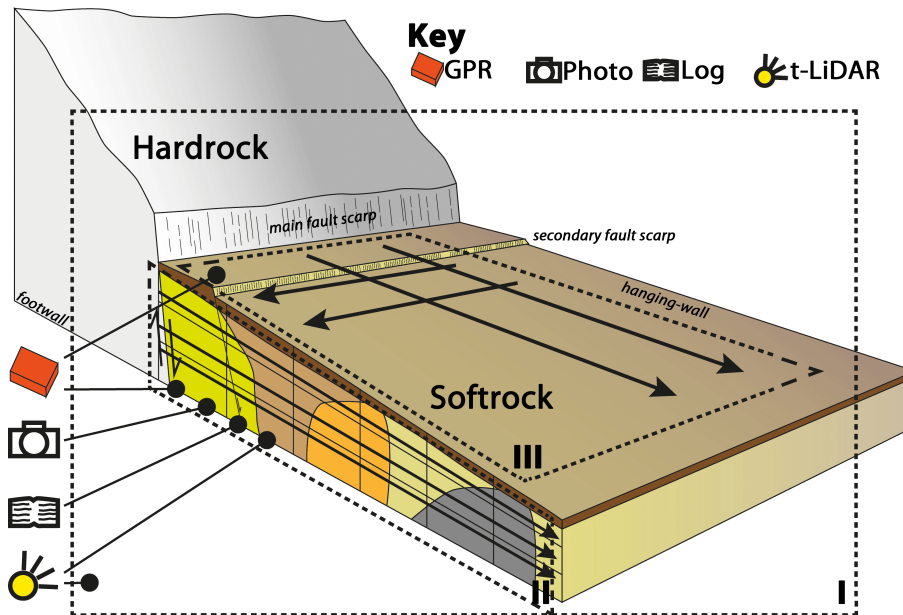


Figure 2. A simplified model of investigated parts on footwall, scarp, hanging-wall, and trench. Dashed lines show the different workspaces: **(i)** overall workspace for a long-mid range t-LiDAR scan to retrieve the geometric relation of investigated components, **(ii)** area of operations (log, photo, t-LiDAR, GPR) on the trench wall, **(iii)** workspace for GPR measurements (black arrows) on top of the colluvium.

Title Page

Abstract

Introduction

Conclusions

References

Tables

Figures

◀

▶

◀

▶

Back

Close

Full Screen / Esc

Printer-friendly Version

Interactive Discussion

An objective multiparametric interpretation of palaeoseismic trench stratigraphy

S. Schneiderwind et al.

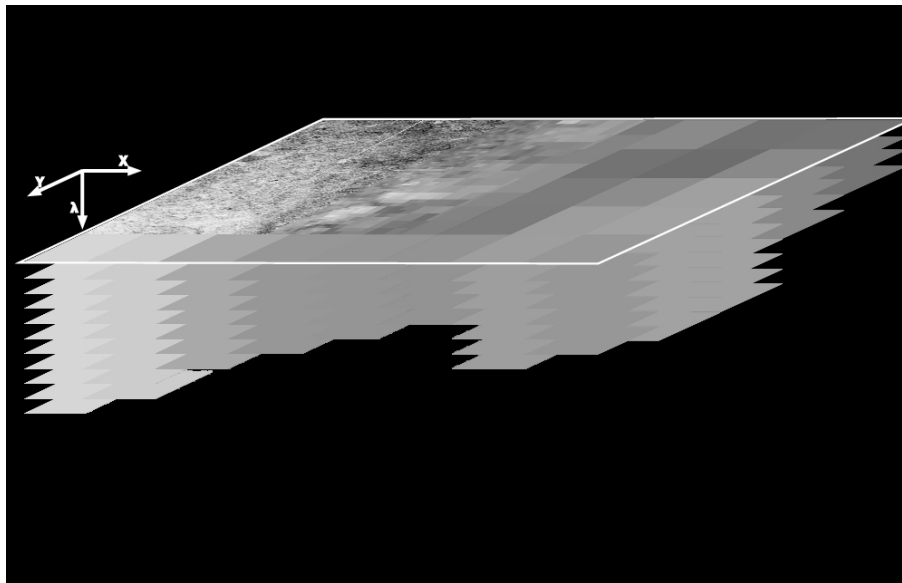


Figure 3. An illustration on how spatial information gets down sampled. The median value of surrounding cells provides the new cell (x, y) value (λ) .

[Title Page](#)[Abstract](#)[Introduction](#)[Conclusions](#)[References](#)[Tables](#)[Figures](#)[◀](#)[▶](#)[◀](#)[▶](#)[Back](#)[Close](#)[Full Screen / Esc](#)[Printer-friendly Version](#)[Interactive Discussion](#)

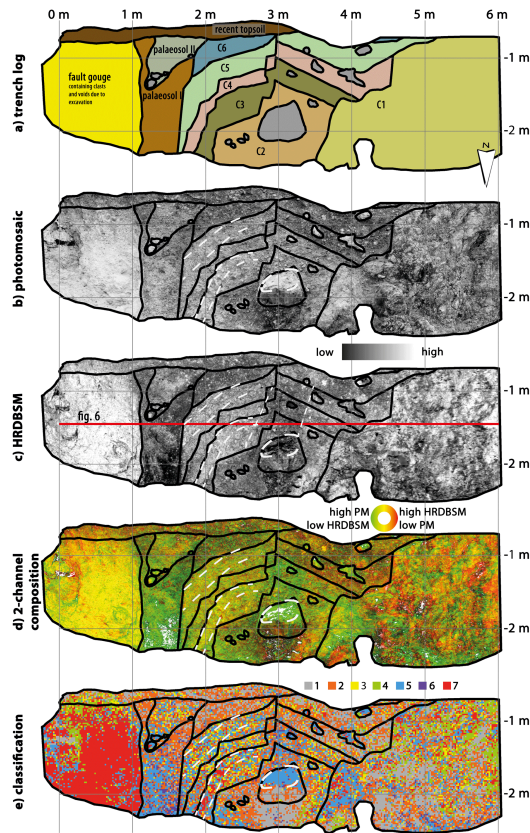


Figure 4. Compilation of analytical input and outcome. **(a)** Trench log produced in the field and corrected with **(b)** photomosaic in the office. **(c)** High-resolution digital backscatter model (HRDBSM) from t-LiDAR measurements. **(d)** Two-channel composition from **(b)** and **(c)**. Note, green and red are 100 % different. (PM = photomosaic). **(e)** Visualisation of spatial distribution of seven classes from the unsupervised classification. White dashed lines indicate coinciding arrangements and some influence from daylight.

An objective multiparametric interpretation of palaeoseismic trench stratigraphy

S. Schneiderwind et al.

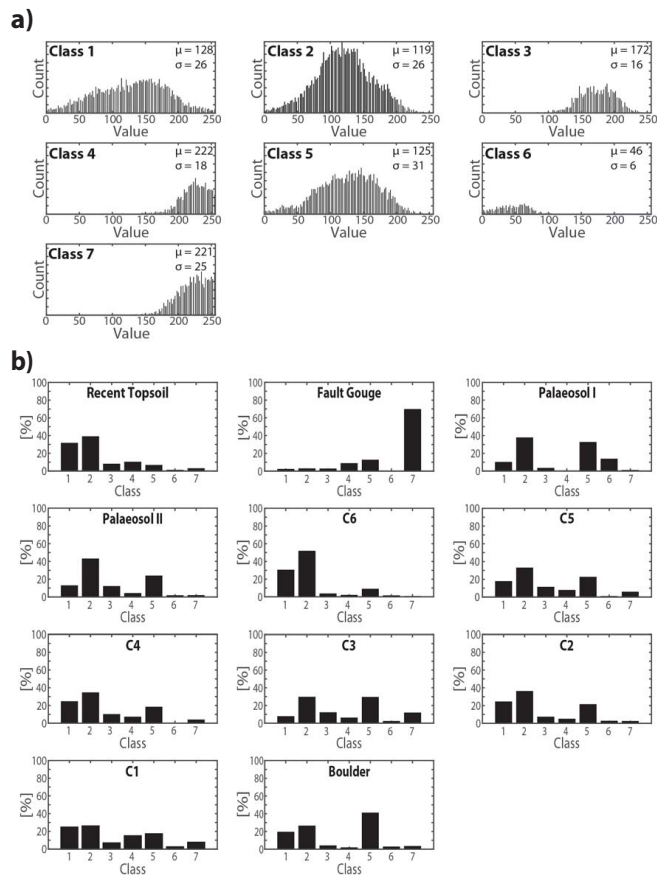


Figure 5. Statistical analysis of two-channel composition image. **(a)** Seven distinct classes were estimated from the unsupervised classification. **(b)** Histograms of representative classes per identified layer. Either the majority of a mapped layer is filled up by one class (e.g. fault gouge) or by a certain composition of 2 or 3 classes (e.g. Palaeosol II and C6).

An objective multiparametric interpretation of palaeoseismic trench stratigraphy

S. Schneiderwind et al.

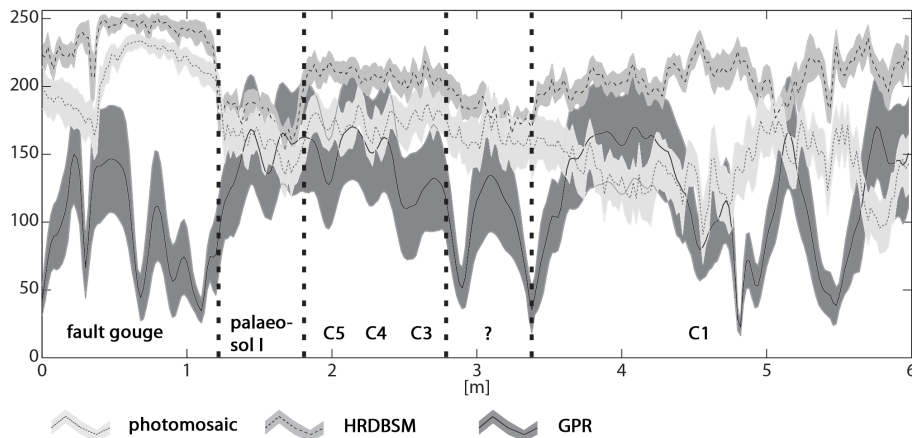


Figure 6. Varying reflectance of electromagnetic waves along the trench wall. Transitions between individual layers are depicted by drastic changing shapes of reflectance spectra. The error bar is given by the standard deviation of each sample.

Title Page

Abstract

Introduction

Conclusions

References

Tables

Figures

◀

▶

◀

▶

Back

Close

Full Screen / Esc

Printer-friendly Version

Interactive Discussion

An objective multiparametric interpretation of palaeoseismic trench stratigraphy

S. Schneiderwind et al.

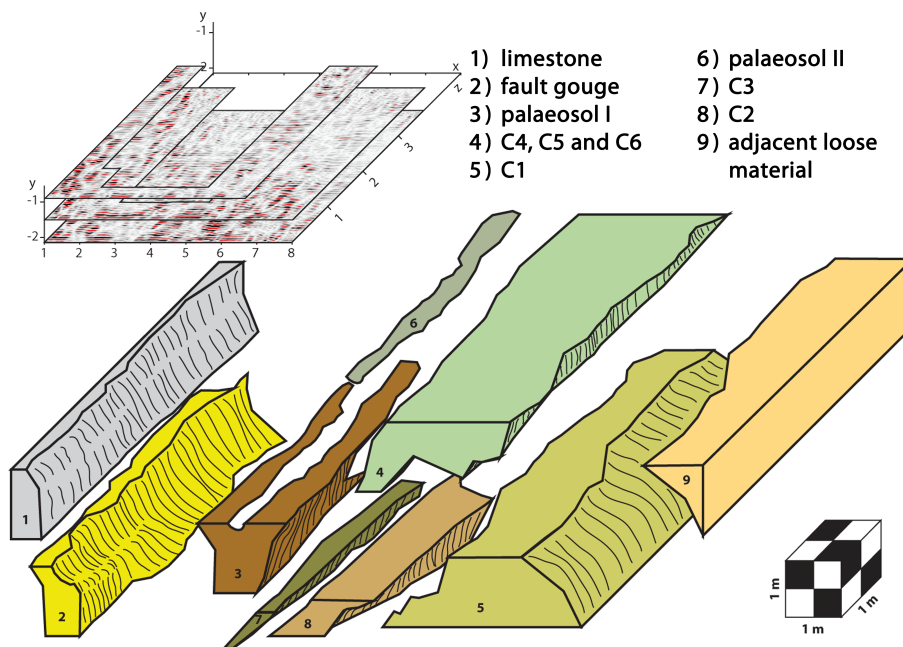


Figure 7. Three-dimensional reconstruction of differing layers within the outcrop from GPR image interpretation. Partial reflection of radar waves on layer contacts leads to significant backscatter signals at depths down to approximately 3 m.

Title Page

Abstract

Introduction

Conclusions

References

Tables

Figures

◀

▶

◀

▶

Back

Close

Full Screen / Esc

Printer-friendly Version

Interactive Discussion

An objective multiparametric interpretation of palaeoseismic trench stratigraphy

S. Schneiderwind et al.

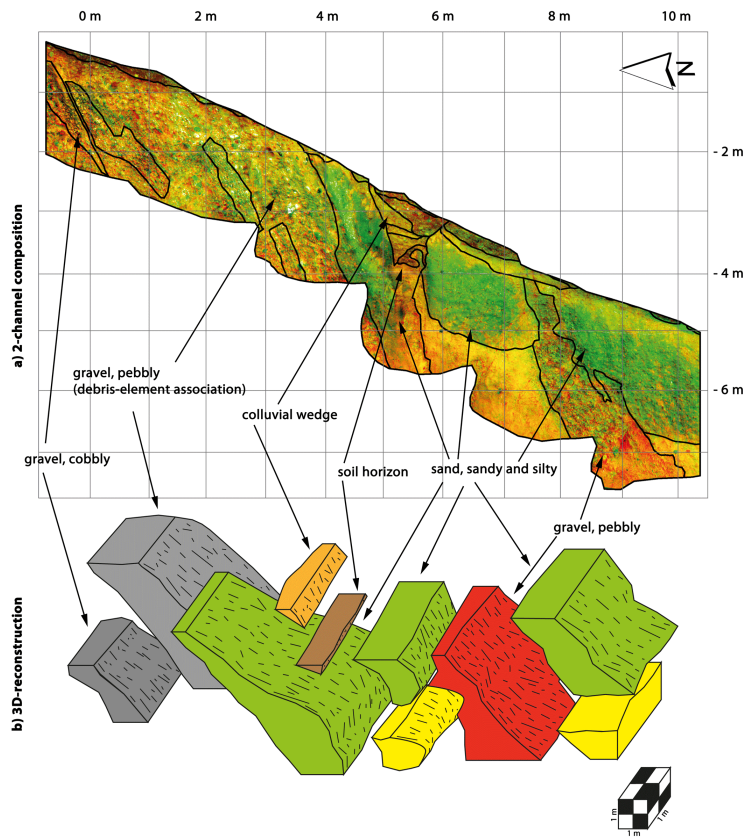


Figure 8. Results from the trenching site of Kokkalas et al. (2007). **(a)** 2-channel composition from multispectral approach. Red and green are 100 % different whereas yellow colouring represents intermediate correspondence of both channels. The trench log (black lines) fits with the multispectral cluster of a certain composition. **(b)** Three-dimensional reconstruction of the trench exposure. Recorded thickness of the colluvial wedge from 1981 is about 0.6 m.

Title Page

Abstract

Introduction

Conclusions

References

Tables

Figures

◀

▶

◀

▶

Back

Close

Full Screen / Esc

Printer-friendly Version

Interactive Discussion